Simplified theoretical model for prediction of catenary action incorporating strength degradation in axially restrained beams

Simplified theoretical model for prediction of catenary action incorporating strength degradation in axially restrained beams

Ofonime Akpan Harry, Yong Lu *

Institute for Infrastructure and Environment, School of Engineering, The University of Edinburgh, Edinburgh EH9 3JL, UK

* Correspondence: yong.lu@ed.ac.uk

Abstract

Catenary action is one of the structural mechanisms that could develop in a laterally restrained beam when subjected to large deformation, and it is a primary mechanism in the resistance to progressive collapse of frame structures in the typical scenario of a column removal. Analytical methods for the analysis of the catenary action exists for idealised beams with simple non-degrading yielding conditions. However, in a realistic beam assembly, especially under a column removal scenario, intermediate failure events such as failure of weld or a bolt at the connection can occur; consequently, the strength of the beam in the plastic region degrades abruptly. This paper presents a simplified theoretical model taking into consideration the degradation of strength in the plastic regions. The basic model is formulated for a generic beam assembly axially restrained with a variable restraining stiffness (flexible axial support), and involves a middle connection. The strength degradation is represented by degraded yield functions. The model subsequently generates a realistic vertical load-deflection relationship, i.e. the resistance function. Comparison of load-deflection relationship so generated with corresponding finite element analysis shows good accuracy. Further comparison of the theoretical model with an existing laboratory experiment also exhibits good agreement. With the generated resistance functions, analysis of the actual dynamic response of beam assemblies in a progressive collapse scenario can be carried out easily using for example the energy method.

Keywords: Axially restrained beam; resistance function; strength degradation; catenary action; progressive collapse

1. Introduction

In the conventional design of steel beams, the capacity of a beam is governed by the flexural behaviour with formation of plastic hinges at critical locations. However, for axially restrained beams catenary action may develop when the beam deflects into a much larger displacement regime and thus help increase the load resistance beyond the flexural capacity. Such additional resistance has been generally recognised as an important mechanism against progressive collapse of frame structures in a typical scenario of a column removal.

A number of dedicated experimental studies on steel and composite beam assemblies with axial restraint have been carried out [1-7]. These studies have confirmed that with adequate axial restraint, following the flexural bending stage, the so-called catenary action can develop resulting in the beam to behave in a cable-like manner and thus helps carry the gravity loads and improve the resistance against collapse. On the other hand, most of the experimental observations also pointed out the fact that various types of local failure events can occur during the course of large deformations, such as rupture of weld or shearing of a bolt at the connection. Such events cause abrupt degradation of the strength, and thus affect the resistance function, i.e. the load-displacement relationship, and the extent to which the catenary effect can actually develop. Such a phenomenon has also been captured in detailed finite element simulations with incorporation of relevant failure mechanisms (see e.g. [7]).

For the evaluation of a beam assembly under a dynamic progressive collapse scenario with an engineering approach, it is essential that a complete resistance function be reliably established first. In spite of the extensive experimental and numerical research as mentioned above, the development of analytical approach to the calculation of the resistance function for axially restrained beam assemblies has remained largely under idealised assumptions. For example, studies by Izzuddin [8] and Li et al. [9] assumed idealised sectional strength properties in the formulation of the catenary effect, whereas strength degradation due to local failure events was not considered. As a matter of fact, most existing analytical models for beam assemblies under a progressive collapse scenario essentially assume that the plastic strength remains available despite very large deformation. As a consequence, the resistance and the development path of the catenary action could be significantly over-predicted.

In this paper, a simplified theoretical model which takes into consideration the degradation of strength in the plastic regions is developed. The basic model is formulated for a generic beam

assembly with a simple support at each end, and axially restrained with a flexible axial support. This model configuration resembles directly the critical part of a double-span beam scenario with the loss of the middle column, i.e., the central part as truncated between the two contra-flexure points in a column removal scenario. Different yield functions (the Moment-Axial force or M-N interaction curves) may be used in the model, and the formulation can also be easily extended to a double beam configuration with plastic hinges at both end regions in addition to the middle location. The model developed herein can be applied to generate realistic resistance functions for both steel and reinforced concrete beam assemblies. The resistance functions can then be employed for the analysis of the response of the beam assembly in a dynamic column removal scenario for the evaluation of the progressive collapse of the frame structure. Standard methods such as the energy method may be used for the dynamic response analysis and will not be covered in this paper.

2. Analysis procedure for a simplified beam model without consideration of strength degradation

Consider a simply supported steel beam with an axial restraint, as shown in Figure 1(a). The axial restraint is represented by elastic axial stiffness (K_a). For a typical scenario of progressive collapse of a frame structure triggered by the loss of a column, this simplified beam model may be considered as a representation of the critical portion of the "double-span" beam between the contra-flexure points, while the middle connection is treated as a rigid joint. All plastic deformations around the connection zones are lumped into the beam plastic region on both sides of the middle joint. At this juncture, it is worth noting that the actual response of a double-span beam assembly in a column removal scenario would involve two end connections, thus the overall resistance of the beam assembly is inevitably dependent upon the properties of the end connections. Furthermore, the location of the contra-flexure points can move as the deformation and catenary action develop. Therefore, the quantitative relationship between the resistance capacity of a beam assembly with restrained pin-ends and a full double-span beam assembly may not be straightforward. Nevertheless, the use of a simply supported beam assembly with one central connection is advantageous for the investigation into the underlying nonlinear and degrading mechanisms of a critical connection and their effect on the resistance behaviour of the beam assembly. For this reason, a simply-supported beam configuration involving a central connection has been adopted in various existing experimental studies on beam assemblies in a

progressive collapse scenario [e.g. 4-7], and this configuration is also adopted in the present study.

The vertical load-displacement behaviour of such a beam assembly with and without strength degradation is schematically shown in Figures 1(b). Four response stages may be identified from the diagrams, namely elastic bending, plastic bending, transient and catenary action stages.

As shown in Figure 1(b), during the initial stage of loading, the beam assembly behaves in flexure. After the elastic stage, the displacement further increases but the resistance may remain flat or with some degree of increase depending upon the flexural hardening behaviour in the plastic region until a plastic hinge forms. For simplicity, in the present discussion the plastic flexural stage is assumed to follow immediately the end of the elastic stage and without hardening.

It is worth noting here that in real structures the flexural stage of response will generally involve an elastic-plastic transition stage with a nonlinear moment-curvature or moment-rotation relationship at the sectional or plastic hinge level. For example, in a steel section this will result in yielding developing at the outer fibre and gradually extending to the inner fibres until reaching full plasticity. The approximation of the yield point and the yield strength is a separate subject which will not be discussed in detail here. In the present model, the elastic-plastic phase i.e. the point between the yield of the outer fibre and the formation of full plastic capacity (denoted as M_p) is simplified into the elastic stage. Plastic hinge only develops at a full plastic moment capacity M_p. With this assumption, the beam can be simplified to have elastic-perfectly-plastic bending behaviour.

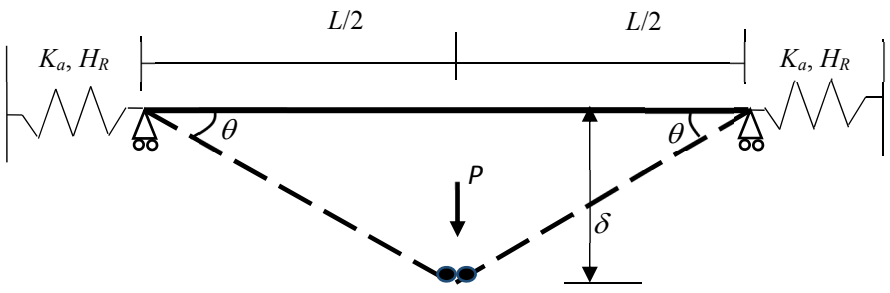

(a) A typical axially-restrained beam assembly with flexible or rigid axial restraint

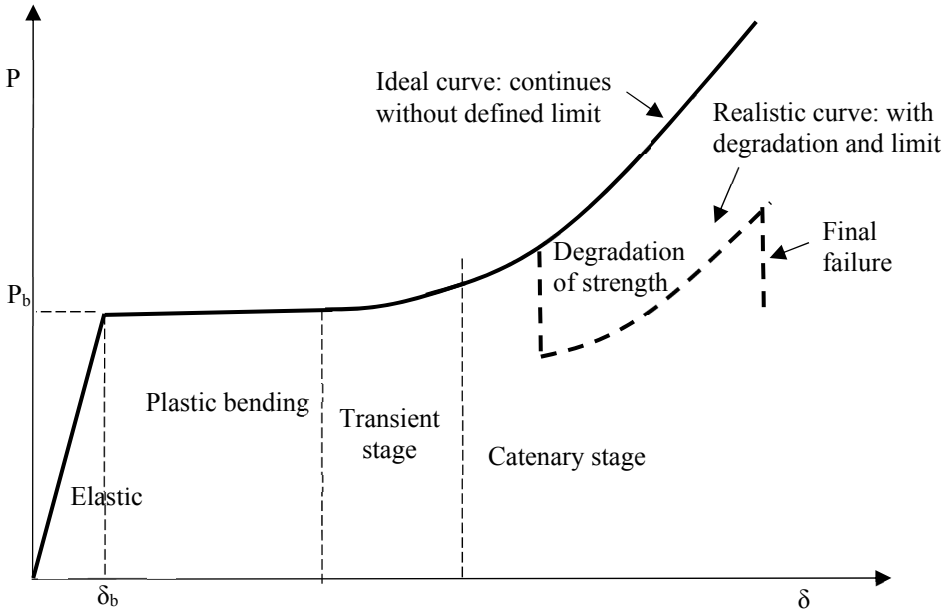

(b) Schematics of load-displacement curves (resistance functions)

Figure 1. Representative axially restrained beam assembly and resistance curves

2.1 Elastic stage

At this stage the beam behaves in a flexural manner and depends on the flexural rigidity and any rotational restraint of the beam. In the basic case, axially-restrained simply supported beam is considered. Plastic hinge will develop at the middle as shown in Figure 1(a). Since this stage involves elastic bending, small deflections are expected, and hence axial force is negligible. The end of the elastic stage is reached once the plastic moment capacity in the critical region(s) is reached. The vertical load and the middle displacement at the idealised yield point are given by:

$$P_b = \frac{4M_p}{L} \tag{1}$$

$$\delta_b = \frac{P_b L^3}{48EI} = \frac{M_p L^2}{12EI} \tag{2}$$

2.2 Transient stage/catenary action stage

In the transient stage, axial tension develops and the behaviour of the beam is governed by a combination of bending moment and tensile force. Thus, there is the stretching of the beam in

addition to bending. Axial force effect needs to be considered. The load-displacement behaviour in this stage is determined incrementally by considering these three key areas [8]:

a. Interaction between the internal forces, i.e. bending moment and axial force (yield function) at the critical section or plastic hinge.
b. Compatibility relationship i.e. the relationship between deformation (incremental axial deformation and plastic rotation) at the plastic hinge and the internal forces which is determined by a flow rule.
c. Equilibrium of the external and internal forces.

Each of these three areas are discussed in the sub-sections that follow.

2.2.1 Yield moment-axial force interaction equation

The plastic interaction function between axial force (N) and bending moment (M) at a beam plastic region is generally nonlinear. A typical N-M interaction curve is schematically shown in Figure 2, and may be expressed by the following equation [10]:

$$\frac{M}{M_p} + \psi \left(\frac{N}{N_p} \right)^2 = 1 \qquad (3)$$

where M and N are the moment and axial force, M_p and N_p are the maximum plastic bending capacity and maximum axial capacity of the section. ψ is a coefficient which depends on the sectional properties. For a rectangular section with perfect plastic condition, ψ is 1 [11]. The interaction of forces, herein bending moment and axial force, in a RC section is much more complex than the case illustrated in this section; however, an expression similar to Equation (3) can also be derived.

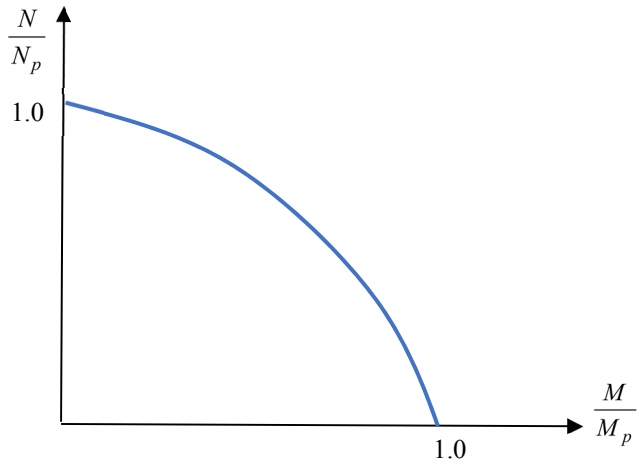

Figure 2: Moment-curvature behaviour at section and plastic hinge

For simplicity, a linear approximation of the interaction curve is often employed (e.g. [8]), and the linearlised relationship may be expressed as:

$$\frac{M}{M_p} + \frac{N}{N_p} = 1 \tag{4}$$

In the present model the general expression in Equation (3) is adopted.

2.2.2 Constitutive relationship between internal forces and deformation

In the theory of plasticity, it is known that for perfectly plastic material, the yield surface remains fixed. Once yielding condition is fulfilled, an infinitesimal increase in stress will lead to plastic flow. The plastic flow obeys a plastic potential function. In the case of associated flow, the plastic potential function coincides with the yield function. Thus, the vector of plastic deformation increment has direction normal to the yield surface. More detail on this can be found in Chen & Han [12]. This concept has been extended to relate internal forces (M, N) to deformation $(d\Delta, d\theta)$ at the plastic hinge zone [9, 13].

Referring to Figure 2, let φ define the yield function, where φ is a function of bending moment and axial force. Since any combination of internal forces (bending moment and axial force) must always lie on the yield surface, it implies that;

$$\varphi = f(M, N) = 0 \tag{5}$$

For each incremental displacement δ_i, the corresponding elongation (u_i) can be determined as:

$$u_i = 2 \times \left(\sqrt{(L/2)^2 + \delta_i^2} - (L/2)^2 \right) \tag{6}$$

Equation (6) can be simplified further and neglecting smaller terms, it gives:

$$u_i = 2\frac{\delta_i^2}{L} \tag{7}$$

The elastic elongation of the beam outside the plastic hinge region then becomes:

$$u_{ei} = u_i - u_{pi} \tag{8}$$

From Hooke's law, the axial force can be related to the effective axial stiffness and elastic axial deformation of the beam as:

$$N = K_e(u_i - u_{pi}) \tag{9}$$

where K_e is the effective axial stiffness of the beam assembly which is defined as:

$$K_e = \frac{1}{\frac{1}{K_a} + \frac{1}{K_s} + \frac{1}{K_a}} \tag{10}$$

where K_a is the elastic axial stiffness of the end spring and K_s is the axial stiffness of the beam ($K_s = EA/L$).

Applying flow rule theory to Equation (5), the incremental axial deformation (du_p) and rotation ($d\theta_p$) occurring at the plastic hinge can be expressed as [13]:

$$\begin{Bmatrix} d\theta_p \\ du_p \end{Bmatrix} = \lambda \begin{Bmatrix} \partial\phi/\partial M \\ \partial\phi/\partial N \end{Bmatrix} \tag{11}$$

where $\partial\phi/\partial N$ is the partial derivative of the yield function with respect to N and $\partial\phi/\partial M$ is the partial derivative of yield function with respect to M. λ indicates the magnitude of plastic deformation.

Equation (11) can be further simplified to:

$$du_p = \frac{\partial\phi/\partial N}{\partial\phi/\partial M} d\theta_p \tag{12}$$

Since the normality condition holds for infinitesimal increments in elongation and rotation, Equation (9) can be re-written in incremental form as:

$$dN = K_e \left(du - \frac{\partial\phi/\partial N}{\partial\phi/\partial M} d\theta_p \right) \tag{13}$$

Noting that for a rigid-plastic beam, the incremental plastic hinge rotation at the mid-span is given as:

$$d\theta_{pm} = 4\frac{d\delta}{L} \tag{14}$$

Also, from Equation (7)

$$du = 4\frac{\delta . d\delta}{L} \tag{15}$$

Substituting Equations (14) and (15) into (13):

$$dN = K_e (4\frac{\delta . d\delta}{L} - \frac{\partial\varphi/\partial N}{\partial\varphi/\partial M} . 4\frac{d\delta}{L}) \tag{16}$$

Assuming the starting deflection is the deflection at the end of elastic bending stage. δ_b, the axial force at any given deflection δ_i can be expressed by integrating Equation (16) from δ_b to δ_i, as:

$$N_i = K_e \left[\frac{2}{L}(\delta_i^2 - \delta_b^2) - \frac{4}{L}(\delta_i - \delta_b) \frac{\partial\phi/\partial N}{\partial\phi/\partial M} \right] \tag{17}$$

Thus, for a given deflection, the corresponding axial force can be calculated using the expression in Equation (17) and subsequently the moment can be determined from the yield function (Equation 5).

2.2.3 Equilibrium of forces

To determine the load at each incremental deflection, one-half of the beam and the forces acting on it are considered as shown in Figure 3. Although the axial force in the beam may slightly differ from the horizontal reaction, experimental test [14] shows that the difference is negligible hence herein the horizontal reaction (H_R) is assumed to be the same as the axial force at plastic hinge which is denoted as (N).

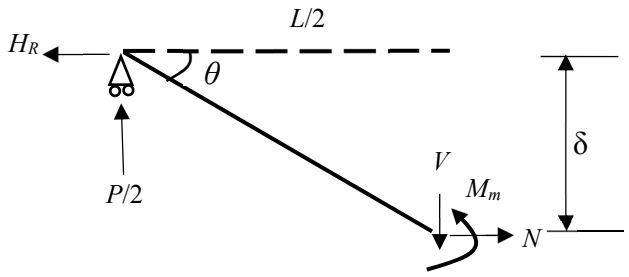

Figure 3: Free body diagram showing forces acting on the beam

Taking moment about the middle point yields:

$$P = \frac{4H_R\delta}{L} + \frac{4M_m}{L} \tag{18}$$

It should be mentioned that the formulation above is in terms of axial and rotational deformation (u and θ). In reality the deformation is concentrated in a small segment of the beam, i.e. the plastic hinge zone with a finite length (L_p). In some cases, such as a steel beam-column connection, the deformation may be concentrated within a small interface area and consequently the behaviour is only determined by the rotation of the beam. In the later section, the application of this model to different connection types and transformation of the axial deformation and rotation to strain measures based on a nominal plastic hinge length will be discussed.

The flow chart for the determination of load - displacement relationship based on the above outlined procedure is shown in Figure 4.

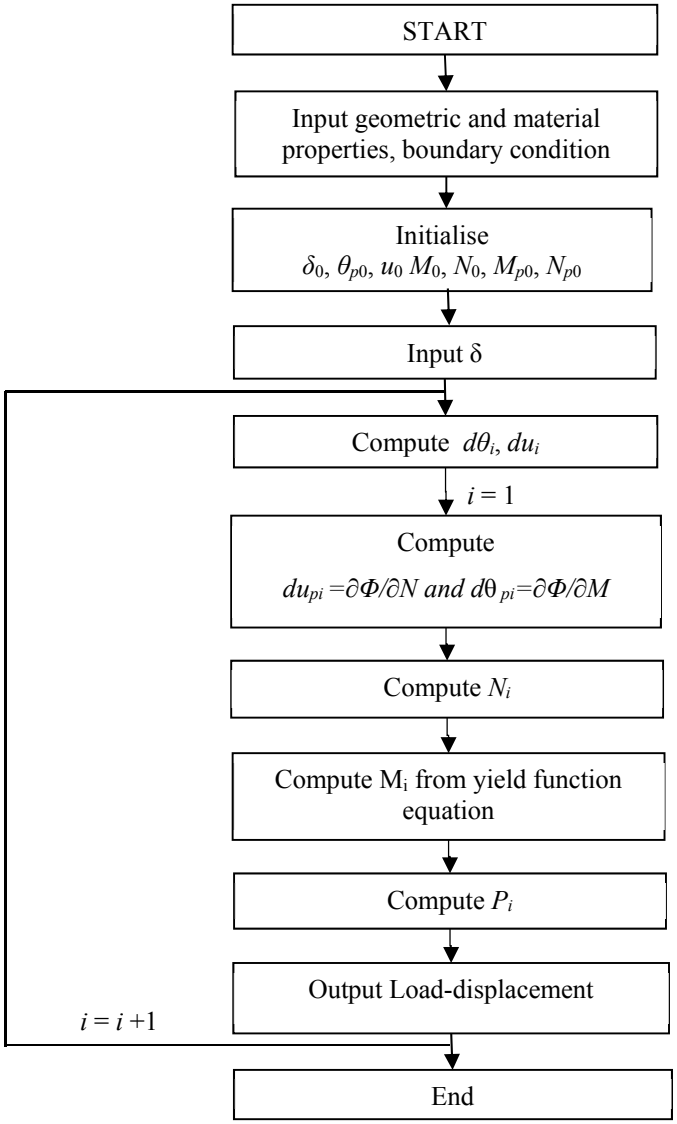

Figure 4: Flow chart for calculating internal forces and vertical resistance without considering strength degradation

3. Illustrative example of finite element simulation and comparison with theoretical prediction without strength degradation

In this section, a 3D rectangular hollow section steel beam is modelled using finite element code (LS-DYNA [15]), and the result is compared with theoretical prediction without strength degradation.

3.1 Finite element model description

The model consists of a two-span beam made of a steel rectangular hollow section. Steel hollow section is selected for the sake of simplicity in terms of lateral stability in the large deflection regime, so as to avoid unnecessary complexities such as torsional buckling in this illustrative analysis. The overall span of the beam is 9.2m (4.6m single span) and depth and width are 300mm by 150mm with a wall thickness of 10mm. Young's modulus and Poisson's ratio of steel are taken as 200GPa and 0.3 respectively, while the yield strength is assumed to be 300MPa.

The beam is modelled with constant stress solid element. A mesh convergence study was performed and a final mesh size of 10 x 5 x 10mm was used across the beam thickness, and 10 x 10 x 10mm was used within the hollow session area. Taking advantage of symmetry, only one-half of the beam is modelled and appropriate boundary condition is applied at the middle column stub of the subassembly.

Pin boundary condition is applied at the end section to simulate the presence of axial restraint from the surrounding structures. To achieve this boundary condition, the end region is modelled with elastic elements so as to avoid localised damage that would increase the complexity of the problem. A hole of 20mm diameter is created within the elastic end region with centre of hole located at the mid-depth of the beam. A rigid rod with the same diameter is created having the same centre as that of the hole. The elastic end is modelled with MAT_001_ELASTIC and the rod is modelled with rigid element MAT_020_RIGID in LS-DYNA. The ends of the rod are constrained in all direction. Interaction between the rod and elastic beam end is defined by a surface-to-surface contact available in LS-DYNA, where the rod surface is defined as the master surface and the elastic beam is defined as slave surface. The FE model of the end region is shown in Figure 5. The top surface nodes of the middle column region are push down in a displacement controlled loading manner. The loading speed is defined small enough to represent a quasi-static loading scheme and thereby avoid any oscillation in the loading process.

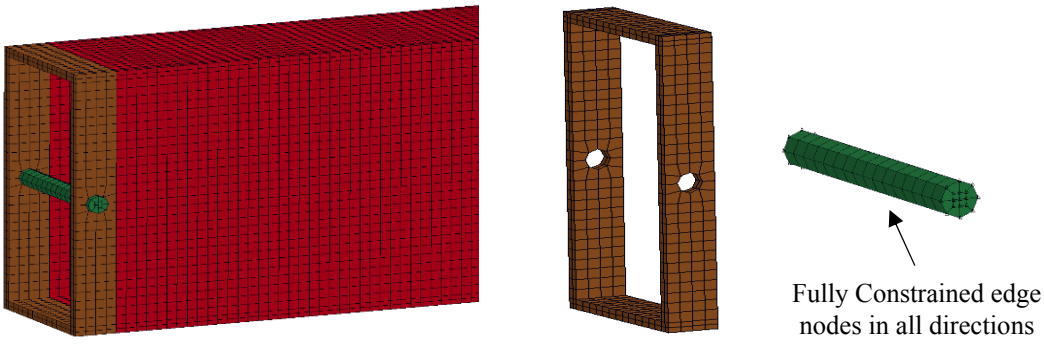

Figure 5: Geometric and boundary details of the FE model: left = part of beam near support; right = pin support

For the theoretical model, the same material and geometric properties used in the FE model is adopted. Without considering the strength degradation, the plastic interaction is defined by the yield interaction curve according to Eq. (3), where the coefficient ψ is approximately equal to 1.12 for a rectangular hollow section. The yield moment (M_p) and axial force capacity (N_p) is calculated as 248 kNm and 2580 kN respectively. The axial stiffness of the end supports (K_a) in the theoretical model is assumed a very large number to represent a rigid axial restraint.

3.2 Results and discussion for FE and theoretical models with no strength degradation

The load-displacement response for the FE and theoretical models is presented in Figure 6. The FE model slightly over-predicts the response compared to the theoretical models and the axial capacity of the beam section is reached at a lower displacement compared to the theoretical model. This is because in the FE model, axial force develops at an early stage prior to formation of the plastic hinge whereas in the theoretical model, axial force is assumed to start after formation of plastic hinge, which occurs herein at a mid-span displacement of 85mm.

The plastic strain distribution along the bottom fibre of the beam at three different middle column displacements of 90, 300 and 500mm which corresponds to start of yielding, transient stage and pure catenary action stage are also shown in Figure 6(b) to shed more light into the evolution of plastic strain and the plastic zone at the middle section of beam.

As illustrated in Figure 6(b), at a middle displacement of 300mm, the maximum plastic strain is about 0.1. For a typical steel connection with welded flange and bolted web (e.g. [6,7,16]) some of the connection components e.g. bottom flange weld may have fractured causing a

reduction in strength. More so the final failure of the connection may occur well before the pure catenary displacement of 500mm is reached. In such cases, using a model with no consideration of strength degradation and eventual failure limit will overestimate the load capacity of the steel assembly under column removal. For the real behaviour to be captured, it is imperative to consider the degradation of the internal forces (axial force and bending moment) caused by the failure of some of the components of the connection and the eventual failure limit. It is on this premise that degradation of the strength is considered in the next section to reflect the actual behaviour as observed in the experiments.

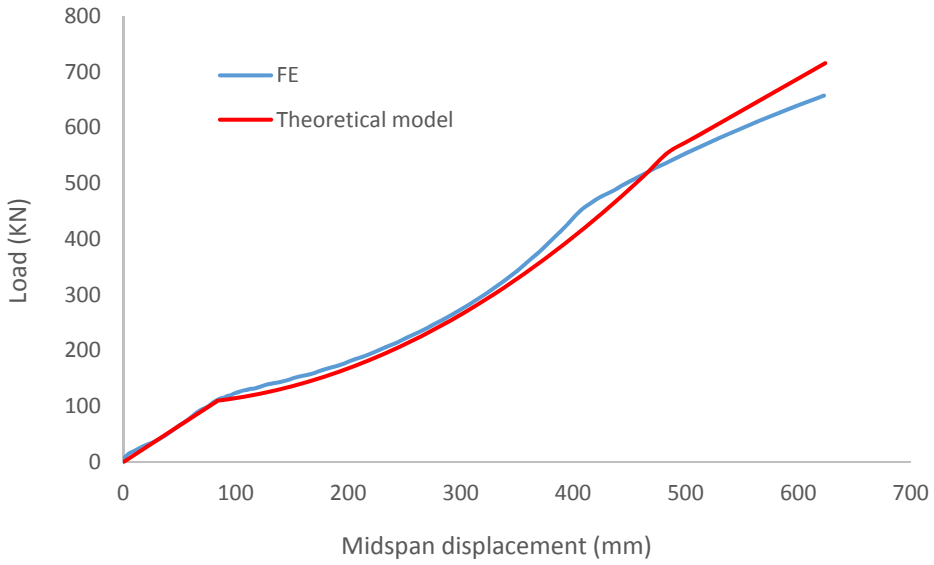

(a) Load-displacement curve for FE and theoretical model without strength degradation

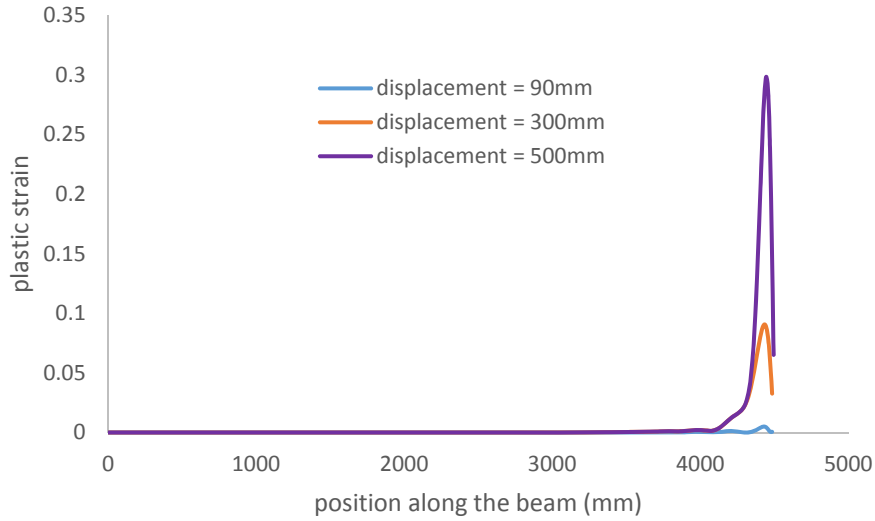

(b) Plastic strain distribution along the beam bottom from FE analysis

Figure 6: Load - displacement functions and local deformation (strain) results

4. Degradation of strength surface

4.1 Concept of strength degradation and implications on catenary effect

The illustration in Section 3 clearly shows the need to incorporate strength degradation in the theoretical model for accurate predictions. In this section incorporation of strength degradation is explained in detail.

To illustrate the concept of degradation of strength, consider a steel connection in Figure 7(a), which is subjected to large downward deformation in a column loss scenario. The connection represents a typical semi-rigid steel connection where the beam flange is welded to the column and the beam web is bolted to the column through the web cleat on each side of the connection.

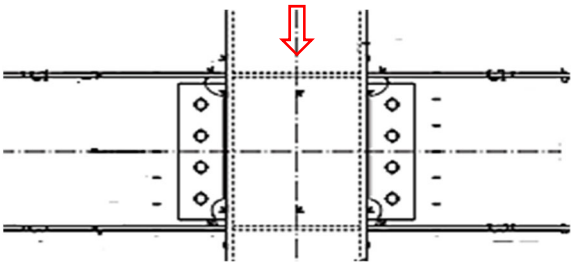

(a) Typical semi rigid steel connection (Li et al. 2015)

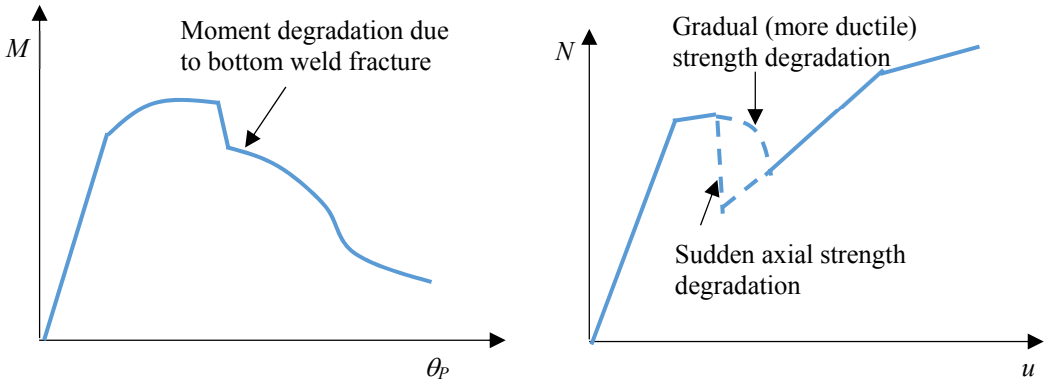

(b) Bending moment-rotation curve (c) Axial force-axial displacement relationship

Figure 1: A representative joint connection and process of strength degradation

At the start of the loading, the beam behaves in flexure with the top flange in compression and bottom flange in tension. As the load increases, the flexural capacity is reached. Further loading

will lead to the fracture of the bottom weld. Once this happens, the flexural and axial capacity of the section is significantly reduced and it is limited by the bolts connecting the beam to column in the web section and the top flange weld. This reduction in the flexural and axial capacities of the connections need to be considered to ensure a more reliable prediction of the global load-displacement response i.e. the resistance function.

As shown in Figures 7(b) and (c), due to the failure of the bottom flange weld, the bending moment and axial force is reduced. The reduction of axial force may be steep or less steep (more ductile, as depicted in Figure 7(c)) depending on the ductility of the welded area.

The M-N curve corresponding to the ultimate and degraded surfaces after failure of the bottom weld are shown in Figure 8. In this theoretical model, the equilibrium is sought for on the degraded surface once the failure criteria are met. The way and manner in which this is done in the model, which is indicated in Figure 8, is explained in the section that follows.

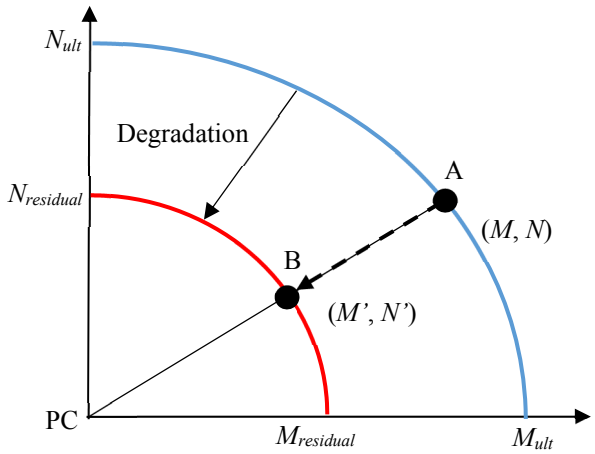

Figure 8: Ultimate and residual yield surfaces

4.2 Implementation of degradation of yield surfaces in the beam analysis procedure

4.2.1 General rules

Given the yield and residual yield surfaces, the reduction of internal forces (bending moment and axial force) can be obtained once the specified failure criteria are reached. As an illustration, Figure 8 is reconsidered. Let A be a point (on the ultimate or maximum yield surface) at which a specified condition for degradation is fulfilled. For further increment, equilibrium is sought for using the residual strength surface. Before seeking for equilibrium on the residual surface,

the internal forces need to be reduced such that a combination of axial force and bending moment lies on the new residual yield surface.

The method of reducing these internal forces belongs to the plasticity theory and there have been different methods to determine the new position on the residual surface depending on the hardening rule used. In this model, the radial method is adopted [17, 18]. According to this method, every point on the ultimate yield surface (or bounding surface) has a corresponding image point on the degraded surface. Any mapping rule adopted must satisfy the identity condition [18]. By identity condition, it means that the new internal forces must lie on the degraded surface.

Using the radial mapping rule, the image of point A(M, N) on the maximum surface is projected onto the degraded surface B(M', N'). This image point can be determined using the following expression [18]:

$$M' = M_c + \mu(M - M_c) \tag{19}$$

$$N' = N_c + \mu(N - N_c) \tag{20}$$

where μ is the ratio between internal forces on the degraded and maximum yield surfaces. M_C and N_C corresponds to the projecting centre (PC). M and N are the internal forces on the maximum yield surface and M' and N' are the corresponding image point on the degraded surface.

In this model, isotropic hardening is assumed. This means that the yield surface can expand or contract (hardened or softened) but cannot translate. Therefore, the projection centre (PC) is fixed. With this assumption, Equations (19) and (20) can be further simplified to:

$$M' = \mu M \tag{21}$$

$$N' = \mu N \tag{22}$$

where M_C and N_C are zero as shown in Figure 8.

The value of μ can be determined by substituting Equations (21) and (22) into the degraded surface function. An example of generalised representation of degraded nonlinear yield function is given in Equation (23) as:

$$\frac{M}{\rho_M M_p} + \psi\left(\frac{N}{\rho_N N_p}\right)^2 = 1 \qquad (23)$$

where ρ_M and ρ_N are the reduction factors for axial force and bending moment.

It should be noted that in the present model, the migration from the initial yield surface to the degraded (residual) strength surface is done instantaneously, which directly represents an abrupt failure event such as fracture of a weld on the flange or shearing failure of a bolt. A more ductile failure event, such as what may occur in some bolted components, could be accommodated by a more gradual migration between the yield and degraded surfaces. Furthermore, for cases where successive degradations may be involved, such as successive failure of bolts, multiple degradation surfaces could be defined. However, such features have not been currently been implemented in the model.

4.2.2 Condition for activating strength degradation

The formulation presented in Section 3 is in terms of rotation as well as axial deformation at the connection. However, defining a rotation criterion upon which strength degradation can occur is difficult as it will inevitably depend on the connection types as well as details, and so far there has been limited research into the quantitative definition of rotational criteria for different types of connections. On the other hand, strength degradation is typically triggered by a local failure event such as fracture of a weld or failure of a bolt component. In this respect it is rational to associate the strength degradation with a local deformation measure resulting from a combination of the axial elongation and rotation of the beam.

There may be different ways to measure the local deformation due to the combined effect, depending on the details of the plastic regions and the damage mechanisms. Nevertheless, as a general representation, the combined maximum strain may be indicative of the local demands and hence the attainment of degradation. For this reason, herein we employ the maximum strain as a limiting criterion for the development into degradation phase.

To relate the strain criterion to the plastic deformation in the beam model, it is necessary to express the two components; axial deformation and rotation in terms of the maximum strain in the critical area (plastic hinge zone). Assuming the strain due to axial deformation over the plastic zone with a nominal (or equivalent) plastic length is uniform, and the maximum strain due to the plastic rotation can be determined as:

$$\varepsilon_{max,\theta_p} = \frac{\theta_p / L_p}{d - x_p} \tag{24}$$

where x_p is the compression depth and $(d-x_p)$ is distance from the extreme tension fibre to the neutral axis under bending alone; for a simple plastic section $(d-x_p)=d/2$.

Combining the axial and rotational effects, the total strain becomes:

$$\varepsilon_{max} = \frac{\sigma_y}{E} + \frac{u_p}{L_p} + \frac{\theta_p / L_p}{d - x_p} \tag{25}$$

where;

ε_{max} is the maximum strain in the plastic hinge, σ_y is the yield strength of the material, u_p is the axial elongation, θ_p is the angular rotation, d is depth of the section, and L_p is a nominal (or equivalent) plastic hinge length.

It should be noted that the actual nominal plastic hinge length would depend upon the connection details and need to be determined from physical experiment or using detailed finite element analysis. This is a subject requiring separate studies and will not be discussed further here.

A flow chart showing the implementation of the strength degradation is given in Figure 9.

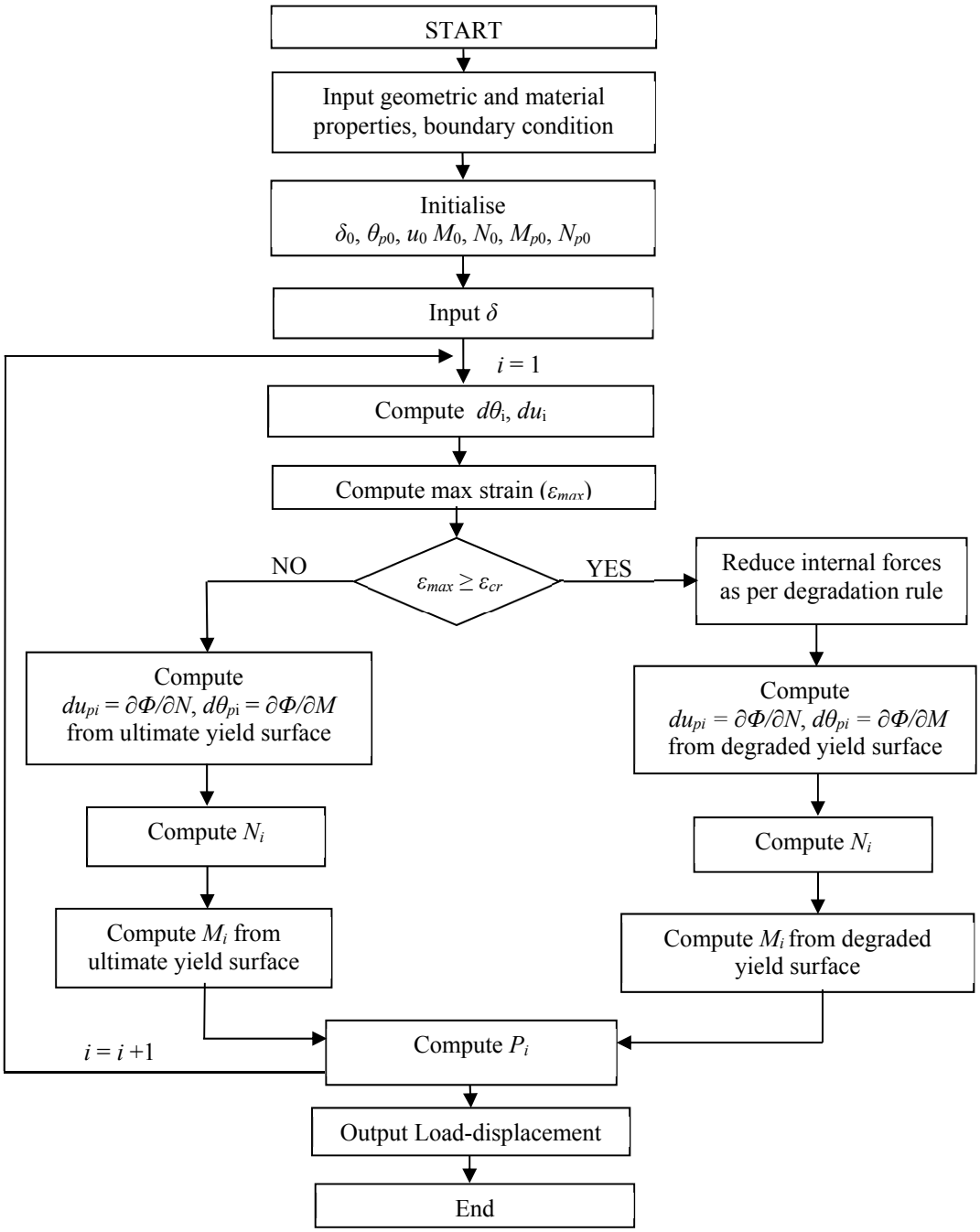

Figure 9: Flow chart for calculating internal forces and vertical resistance with consideration of strength degradation

5. Verification of the theoretical model for prediction of load-displacement resistance function with strength degradation

5.1 Validation with a conceptual FE simulation

The same beam modelled in Section 3 is considered here. For simplicity in this illustration, the beam is modelled with elastic-perfectly-plastic material properties with yield strength of 300MPa. The strength degradation is conceptually represented by a reduction of the beam section in the critical zone, simulating a local failure event such as a weld failure. For this purpose, an area near the middle joint (where the lower column is missing) is created with 50mm in depth and 100mm in length, and this area is modelled with another material of the same property (elastic-perfectly-plastic with yield strength of 300MPa) but will rupture when the maximum strain reaches a specified failure strain of 0.1. When this happens, the elements in this section being will be eroded which leads to the degradation of strength. Figure 10(a) shows the FE model, where the critical section with failure strain of 0.1 can be seen adjacent to the beam-joint interface. The schematic representation of the section before and after strength degradation is shown in Figure 10(b-c).

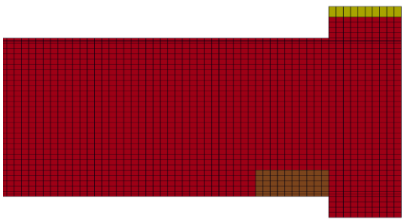

(a) FE model with degraded area

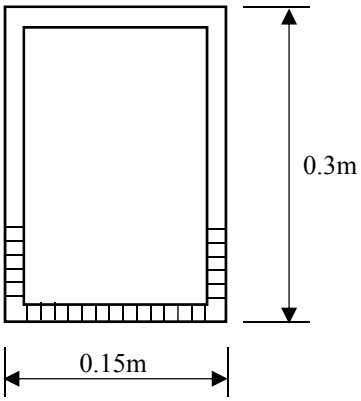

(b) Intact Section

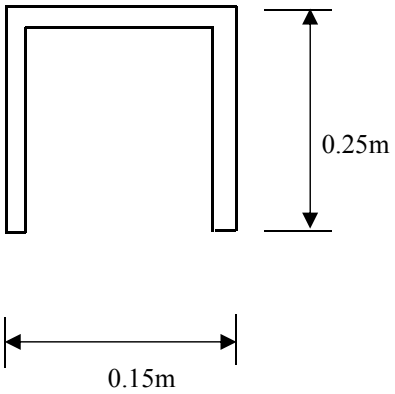

(c) Section after partial failure

Figure 2: Illustrative example with strength degradation in critical region

For the undamaged section used in this analysis, the bending moment-axial force interaction is governed by the equation:

$$\frac{M}{M_p} + \psi\left(\frac{N}{N_p}\right)^2 = 1 \qquad (26)$$

To determine the degraded yield surface, three points were selected to calculate the axial force and bending moment using the degraded section in Figure 11(c). These included;

1) Section in pure bending (no axial force).
2) Section subjected to axial force without bending and,
3) A combination of certain amount of axial force and bending moment

Based on these three points, interaction curve for the full and degraded yield surfaces are shown in Figure 11.

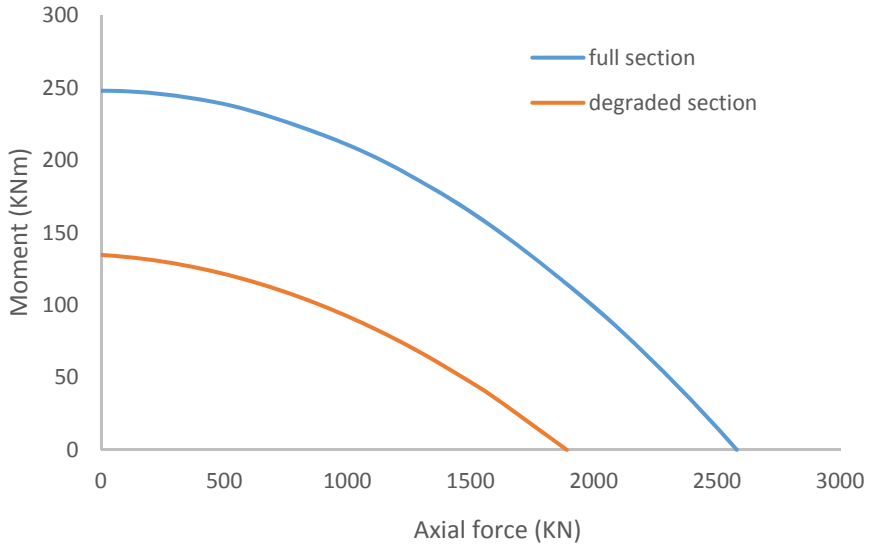

Figure 3: Moment-axial force interaction curves for full and degraded sections

The equation for the normalised relationship between bending moment and axial force for the degraded surface can be expressed as:

$$\frac{M}{M_{p1}} + 0.86\left(\frac{N}{N_{p1}}\right)^2 + 0.14\left(\frac{N}{N_{p1}}\right) = 1 \qquad (27)$$

where M_{p1} and N_{p1} are the moment and axial force capacities for the degraded section calculated as 134.6KNm and 1890KN respectively. Noting that the moment (M_p) and axial force (N_p)

capacities for the full section are 248KNm and 2580KN, the moment - axial force interaction in Equation (26) can be expressed in terms of capacities of the full section (M_p and N_p) as:

$$\frac{M}{\rho_M M_p}+0.86\left(\frac{N}{\rho_N N_p}\right)^2+0.14\left(\frac{N}{\rho_N N_p}\right)=1 \qquad (28)$$

where ρ_M and ρ_N are 0.54 and 0.73 respectively.

The comparison of load-middle column displacement between the proposed theoretical model and FE model is shown in Figure 12. It can be seen that the theoretical model captures accurately the reduction in the global strength caused by the failure of elements in the critical section. It should however be noted that the spread of damage zone has an effect on the global load-displacement behaviour. It can also be seen that without accounting for the strength degradation the resistance of the beam assembly would be considerably over-predicted. The exploration herein therefore confirms the importance of capturing the degradation of strength in the critical region on the prediction of the global behaviour of the beam assembly in the large deformation regime.

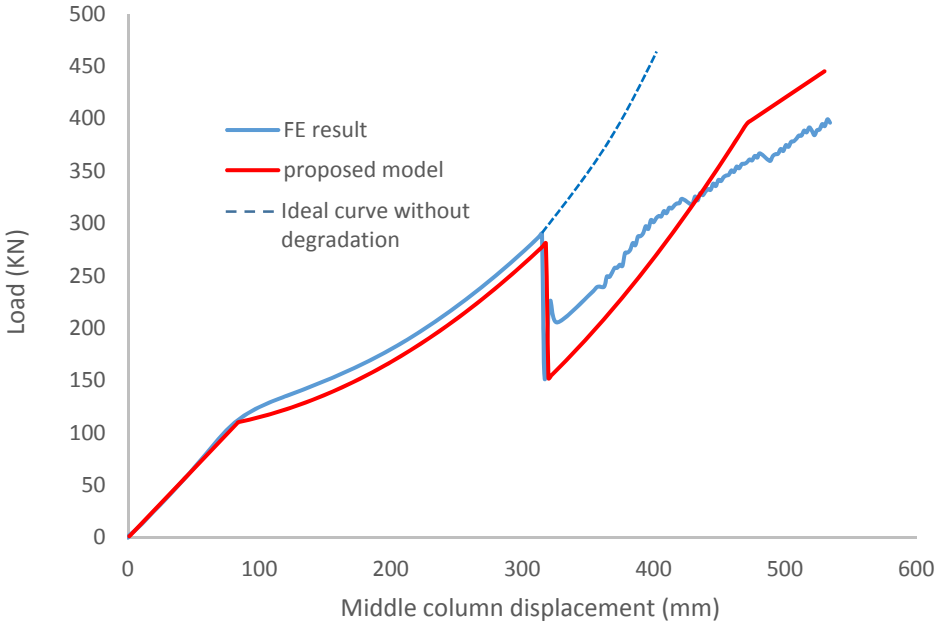

Figure 4: Comparison of load-displacement response from FE and proposed model with strength degradation

5.2 Validation with experiment

The reliability of the theoretical model with strength degradation is further checked using experimental study by Li *et al.* (2015). The steel subassembly tested in their study was extracted from a framed building, taken from the points of contra-flexure in a middle column removal scenario. The detail of the middle beam-column connection as shown in Figure 13 consisted of a beam web bolted to the column through cleat plates and the beam flange welded to the column. Fixed pin supports were applied at the ends of the beam to simulate the axial restraint and the total length of the beam assembly was 4500mm. The beam was made of standard H section H300 × 150 × 6 × 8 ($H \times B \times t_w \times t_f$) and the middle column section dimension was square hollow section (SHS) of size 250 x 14 (D x t). Four rows of bolt were used to connect the beam web to the column. The yield and ultimate material strength of the beam section was 407 and 653MPa respectively. More details about the experiment can be found in Li et al. [7].

As stated previously, the failure criteria for steel subassembly may be well represented by the rotation of the connection. The rotation at rupture of weld and rotation at eventual failure for a given type of joint details may be determined using more detailed studies including physical experiments. Such data from experimental and other studies on limiting criteria can be easily employed in the proposed theoretical model for the evaluation of the load-displacement resistance function. Since such general data is not currently available, herein the rotation corresponding to the rupture of bottom weld and final failure reported in the test is used.

For a more accurate determination of moment-axial force strength curves, a detailed analysis may be performed for the connection before and after the failure of the bottom flange weld taking into consideration of the bolt arrangements. For the present purpose, a simplified analysis of the M-N relationship is performed using an equivalent beam section. The equivalent section for the calculation of M-N curve before and after the rupture of the bottom flange weld is assumed to be the full cross-section and the cross-section without the bottom flange, respectively. This is because after the failure of the weld, the bottom flange no longer contributes to the resistance.

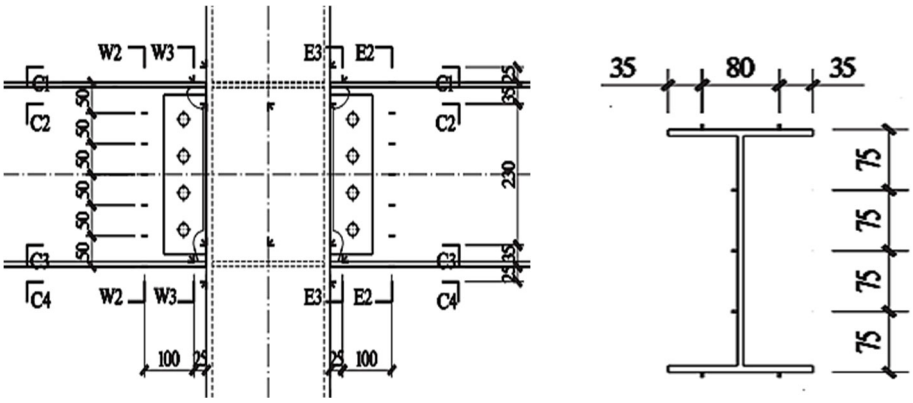

Figure 13: Middle beam-column joint and section details of tested specimen (Li et al. 2015)

The M-N interaction curve for the section before and after bottom weld rupture based on the simplified approach explained above and the section geometry is shown in Figure 14.

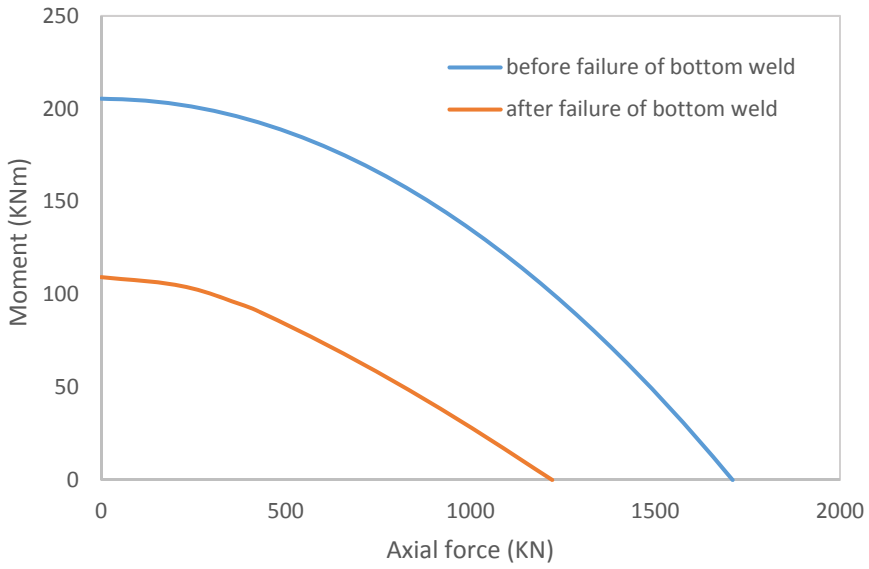

Figure 14: Moment-axial force curves before and after fracture of bottom weld

From Figures 14 the moment-axial force interaction equations for the full and reduced section following bottom weld fracture can be expressed as:

$$\frac{M}{M_p}+\left(\frac{N}{N_p}\right)^2=1 \qquad (29)$$

$$0.98\frac{M}{M_{p1}}+0.69\left(\frac{N}{N_{p1}}\right)^2+0.33\left(\frac{N}{N_{p1}}\right)=1 \qquad (30)$$

where M_{p1} and N_{p1} are the moment and axial force capacities for the reduced section calculated as 109KNm and 1221KN respectively.

The Moment (M_p) and axial force (N_p) capacities for the full section is calculated as 205KNm and 1709KN respectively, hence the moment-axial force interaction in Equation (30) can also be expressed in terms of capacities of the full section (M_p and N_p) as:

$$0.98\frac{M}{\rho_M M_p}+0.69\left(\frac{N}{\rho_N N_p}\right)^2+0.33\left(\frac{N}{\rho_N N_p}\right)=1 \qquad (31)$$

where ρ_M and ρ_N are 0.53 and 0.71 respectively.

Using the maximum and degraded yield surfaces, the load-displacement response is predicted and Figure 15 shows the comparison between the experimental result and the theoretical prediction. It is seen that the theoretical prediction matches well with the experimental load-displacement curve. As mentioned previously, information about the rotation at failure of the bottom weld was adopted from the experiment. If such information is available for a given type of connection, the same procedure can be used to evaluate the global resistance function accordingly.

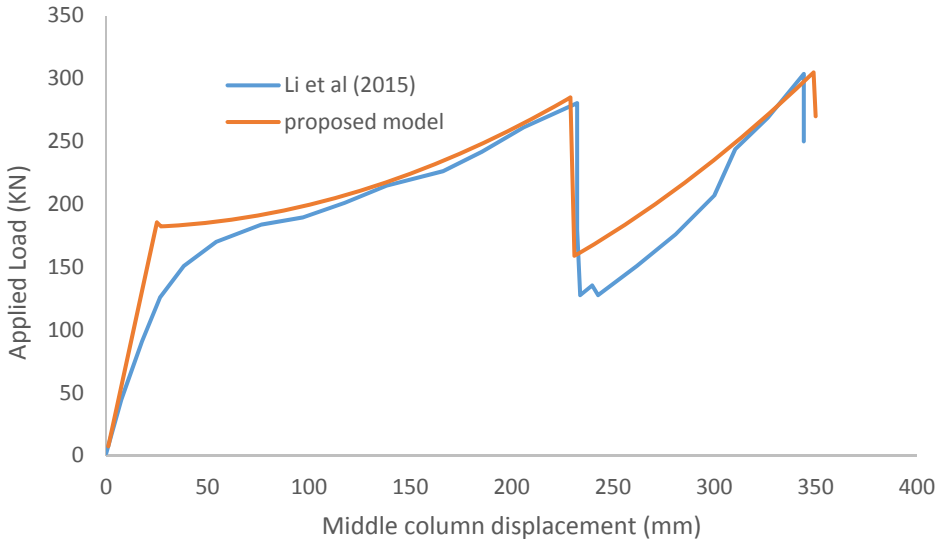

Figure 15: Comparison of load-displacement relationship (resistance function) between experimental result and theoretical prediction

6. Conclusions

This paper presents a simplified theoretical model for the determination of the resistance function in laterally restrained beams, with particular consideration of the strength degradation at the critical plastic regions in the form of degradation of bending moment - axial force (M-N) yield functions. The incorporation of the strength degradation allows a realistic representation of intermediate failure events in the critical region such as a weld failure.

The proposed theoretical model has been verified by comparing the predicted resistance function, i.e. the load - displacement relationship, with finite element simulation and a physical experiment. The comparison shows good agreement and these demonstrate that the model is capable of predicting the global resistance function in a realistic manner.

It should be noted that the application of the theoretical model requires the availability of the M-N interaction relationship for the intact yield state and the residual (degraded) state, as well as the corresponding failure criteria. As can be understood, for different types of beams and connections, the yield functions will be different and these need to be generated separately as part of the section/connection properties. Furthermore, there is still only limited quantitative information in the literature concerning the criteria for local failure events, such as limiting rotation parameters. In fact, such criteria would need be made available for any substructure models using a beam-column analogy. In this respect, further research, both experimentally and numerically (e.g. using detailed finite element models), will be required. Nevertheless, the proposed model in this paper provides a workable framework to take the degradation into consideration in the prediction of the global resistance functions. The framework has been implemented in this paper in a simplified beam assembly involving one (central) connection, and can be extended to full double-beam assemblies with a modified computational procedure. The resistance functions so predicted can subsequently be applied in an analytical procedure for the evaluation of the response of the beam assembly in a dynamic column removal scenario.

Acknowledgement

The authors gratefully acknowledge the funding provided by Niger Delta Development Authority (NDDC), Nigeria, for the PhD study of the first author.

References

[1] Dinu, F., Marginean, I., Dubina, D. Experimental testing and numerical modelling of steel moment-frame connections under column loss. Engineering Structures, 2017; 151: 861–878.

[2] Guo, L., Gao, S., Fu, F. Structural performance of semi-rigid composite frame under column loss. Engineering Structures, 2015; 95: 112–126.

[3] Sadek, F., Main, J.A., Lew, H.S., Bao, Y. H. Testing and analysis of steel and concrete beam-column assemblies under a column removal scenario. Journal of Structural Engineering, 2011; 137(9): 881–892.

[4] Yang, B., Tan, K.H. Experimental tests of different types of bolted steel beam-column joints under a central-column-removal scenario. Engineering Structures, 2013; 54: 112–130.

[5] Yang, B., Tan, K.H. Behavior of composite beam-column joints in a middle-column-removal scenario: experimental tests. Journal of Structural Engineering, 2014; 140(2): 4013045.

[6] Li, L., Wang, W., Chen, Y.Y., Lu, Y. Experimental investigation of beam-to-tubular column moment connections under column removal scenario. Journal of Constructional Steel Research, 2013; 88: 244–255.

[7] Li, L., Wang, W., Chen, Y.Y., Lu, Y. Effect of beam web bolt arrangement on catenary behaviour of moment connections. Journal of Constructional Steel Research, 2015; 104: 22–36.

[8] Izzuddin, B.A. A simplified model for axially restrained beams subject to extreme loading. International Journal of Steel Structures, 2005; 5(5):421–429.

[9] Li, G., Wang, K., Liu, Y., Chen, S. Catenary action of restrained steel beam against progressive collapse of steel frameworks. J. Cent. South Univ. Technol. (Engl. Ed.), 2008; 15(6): 830–834.

[10] Yin, Y.Z. & Wang, Y.C. Analysis of catenary action in steel beams using a simplified hand calculation method, Part 1: theory and validation for uniform temperature distribution. Journal of Constructional Steel Research, 2005; 61(2): 183–211.

[11] Jirasek, M., Bazant, Z.P. Inelastic Analysis of Structures, 1st edition, 2001, John Wiley & Sons.

[12] Chen, W., Han, D. Plasticity for Structural Engineers. 1988, Springer-Verlag, New York.

[13] Long, H. Van, Hung, N.D. Second-order plastic-hinge analysis of 3-D steel frames including strain hardening effects. Engineering Structures, 2008; 30(12): 3505–3512.

[14] Yu, J., Tan, K.H. Structural Behaviour of RC Beam-Column Subassemblages under a Middle Column Removal Scenario. Journal of Structural Engineering, 2013; 139(2): 233–250.

[15] Yang, B., Tan, K.H. Robustness of bolted-angle connections against progressive collapse: experimental tests of beam-column joints and development of component-based models. Journal of Structural Engineering, 2013, 139(9): 1498–1514.

[16] LS-DYNA keyword user's manual version 971. Livermore Software Technology Corporation, 2007.

[17] Dafalias, Y.F., Herrmann, L.R. Bounding surface plasticity. II: application to isotropic cohesive soils. Journal of Engineering Mechanics, 1986; 112(12): 1263–1291.

[18] Seidalinov, G., Taiebat, M. Bounding surface saniclay plasticity model for cyclic clay behavior. International Journal for Numerical and Analytical Methods in Geomechanics, 2014; 38:702–724.